A Novel Seesaw Swivel Actuator Design and Fabrication

Po-Chien Chou, Yu-Cheng Lin, and Stone Cheng

Department of Mechanical Engineering, National Chaio Tung University, Hsinchu 300, Taiwan, R.O.C.

Many small form factor optical pickup heads based on the swing arm design utilize piezoelectricity or slim plate of metal to perform focusing action. The seesaw type actuator is a new driving mechanism used for swiveling the entire optical pickup heads devices. The configuration of the seesaw swivel actuator has unique features including a rotary actuator for coarse and fine tracking and a seesaw arm for swiveling along a pivot instead of a hinge to permit a tilt focus movement. In this paper, a biaxial voice coil motor (VCM) combining the swing type tracking VCM and seesaw type focusing VCM in the rear of the swing arm is proposed. This seesaw swing arm actuator is fabricated and evaluated in dynamic experiments. The performance of the biaxial VCM is verified through simulation by finite-element methods, and the effectiveness is confirmed by experimental procedures and parametric design optimization.

Index Terms—**Multisegmented magnet arrays, seesaw swing arm actuator, small form factor optical head, VCM.**

I. Introduction

OPTICAL disk drive is one of the most popular systems of information storage. Track pitch in Blu-ray (BD) disc adopts 0.32 μm and will reduce to 30 nm for future optical near-field magnetic-hybrid recording. The slider head will run in a flying height of 20 nm. Such a high track density and accurate focusing operation requires a higher precision servo system. The micro-optical disk drive (ODD) can be a solution for compact size and portability [1], [2]. The major trends in enhancing recording density in optical drives rely on combining blue-laser diodes (short wave-length) and high numerical aperture (NA) lens integrated in a micro mechanical head actuated by a swing arm servo system. In order for a swing arm to be successfully implemented in the optical drive, the tracking and focusing movement need to be properly designed to ensure adequate performance of the actuator such as moving stability and tracking servo bandwidth.

In a design of miniaturized swing arm actuator, most research works have focused on the micro-optical system design to meet the optical characteristics, but not many research works discuss the mechanical characteristics about optical head actuator. A swing arm type rotary actuator has advantages over a linear actuator in terms of fast access time, slim shape design, mobility, and high mechanical performance [3], [4]. The swing arm actuator consists of a swing arm, voice coil motor (VCM) of focusing and tracking, and bearing. Many papers on slider design or improvement for ODD and conventional HDD systems have been introduced so far [5]–[8]. However, many important mechanical issues on the design of suspension, swing arm air gap between magnets and yoke have not been discussed in the literature. In Dataplay's patents and some typical focusing mechanism design, the hinge type is actively controlled to the use of VCM for the focusing motion [9]. However, the hinge's metal characteristics make it fragile, leading to failure by fracture in the repeatedly working conditions. In order to improve the disadvantage of the suspension hinge, the seesaw movement takes a fine solution to replace the hinge spring action.

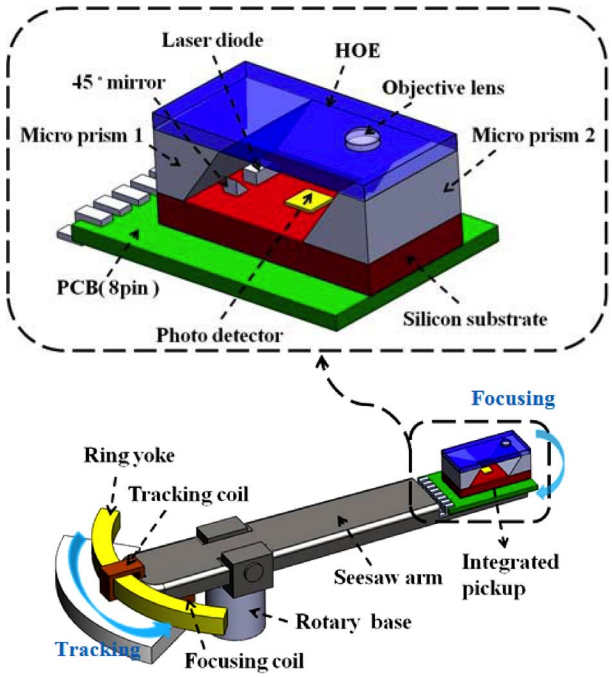

Fig. 1. Schematic diagram of micro-optical pickup head configuration.

In the development of optical drives, a special requirement concerning the flying head consists in the use of very small, lightweight components to have a compact mechanical system. This system adopts a finite-conjugate objective lens with $\mathrm{NA} = 0.65$ for 654-nm laser wavelength. Fig. 1 shows the optical configuration based on the parameters in Table I. A holographic optical element (HOE) is used for simplifying the optical configuration which provides a better approach for alignment [10]. This optical construction can be applied to high density blue-ray storage and holographic optical storage of small form factor in the immediate future [11], [12]. We also designed a seesaw mechanism of the swing arm rotary type actuator system. The seesaw actuator was designed on the basis of electromagnetic (EM) and finite-element (FE) structural analyses for both focus/tracking actuations. Each mechanical part is designed so as to

Manuscript received August 20, 2009; revised February 21, 2010; accepted February 24, 2010. First published March 22, 2010; current version published June 23, 2010. Corresponding author: S. Cheng (e-mail: stonecheng@mail.nctu.edu.tw).

Color versions of one or more of the figures in this paper are available online at http://ieeexplore.ieee.org.

Digital Object Identifier 10.1109/TMAG.2010.2045388

TABLE I
RED LASER OPTICAL PICKUP SPECIFICATIONS

Item	Correspondence
Image object relation	Finite-conjugate system
Laser wavelength	654 nm
Object NA (laser side)	0.1
Image NA (disk side)	0.65
Focal length	0.525 mm
Clear aperture diameter	1.0 mm

satisfy the servo performances and dynamic characteristics [13], [14]. To maximize the seesaw actuator driving force, the magnetic circuit with a fan-shape type magnet for the tracking motion was suggested. In particular, three fan-shape magnets assembly and a unique ring tracking yoke are used in the magnetic circuit. Numerical simulations of optimization and experiments are also realized to evaluate the performance of biaxial motion.

II. DESIGN OF SEESAW TYPE VCM ACTUATOR

In the development of optical drives, especial requirement for the optical flying head is that its components be small and thin enough for the compact mechanical system. With these considerations, the swing arm optical system generally contains high performance electro-mechanical components and actuating mechanism.

Referring to Fig. 2, Dataplay's small form factor disk drive with the swing arm type actuator [15], the overall rotary system consists of pickup head, suspension, hinge spring, and VCM parts. The optical module with high NA objective lens is mounted on the front suspension of carbon fiber arm assembly, and the hinge springs connected the suspension with pivot arm. The hinge spring is actively controlled by the VCM for focusing (focusing coil in Fig. 2) and the suspension is designed for stable tracking and focusing performance of the swing arm. The fine tracking and the coarse seeking are achieved by the VCM for tracking (tracking coil in Fig. 2). The tracking path becomes a curve line of swing arm rather than a straight line of linear motor. Focus motion are achieved by the coil shown at the center of the front suspension [16]. Several approaches are also available to utilize this swing arm type to realize the micro storage system [17]–[19]. In order to improve the structural properties of the swing arm, a triple layer structure of steel-aluminum-steel is used as one of the solutions. Although this structure provides the swing arm with high heat thermal conductivity, the module still requires longer working time to manufacture, which increases the product cost. Furthermore, the concentration of stress between suspension and swing arm result in a loss of mechanical durability. The hinge springs are fragile in the repeated working condition and lead to permanent fracture.

Accordingly, we improve the actuator suspension from two points of view. One is to increase the critical modes of the second torsion mode as they limit the servo bandwidth of the actuating range, and the other method is to decrease the front loading mass for robustness against the hinge spring stress concentration. From a mechanical point of view, the properties of hinge spring rate, ballasting weight have effects on the shock resistance of the suspension. To increase the swing arm actuator

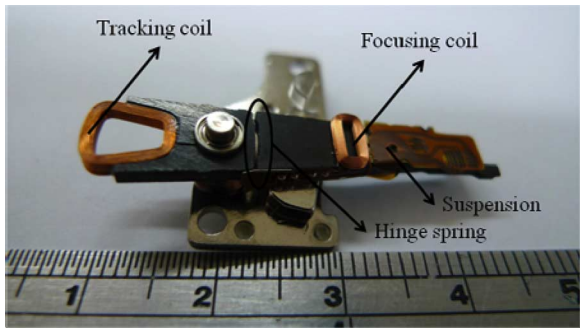

Fig. 2. Dataplay's swing arm actuator.

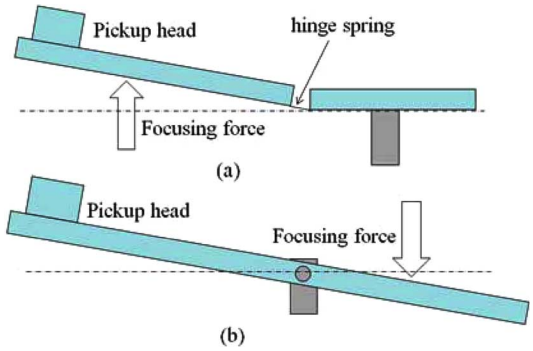

Fig. 3. Two types of focusing mechanism. (a) Upward focusing force is generated by the focusing coil placed beneath the arm (shown in Fig. 2). (b) The focusing coil is placed at opposite side of pivot axial base (shown in Fig. 1), and generated downward focusing force. (a) Hinge spring type. (b) Seesaw type.

resonance frequency, three methods are commonly applied: 1) use the high Young's modulus material such as titanium alloy, however, this makes the machining of the material more difficult; 2) strengthen the stiffness of load suspension with embossments to approach the shape optimization of suspension; and 3) remove the high kinetic energy region of mass.

Schematics of the hinge spring and of the seesaw focusing mechanisms types are shown in Fig. 3, for comparison. In order to improve the fragile hinge spring, a seesaw type rotary VCM actuator without hinge spring is designed for the miniaturization and fine focusing motion. A seesaw is an accurate lever's machine that magnifies force. This is comprised of a suspension (lever arm) and a pivot axial base (fulcrum). The fulcrum is located between the effort force and the load force on the lever arm. The effort force creates a torque around the fulcrum, and this torque is dependent on the magnitude of the VCM driven force and the distance from the fulcrum to the focusing coil. This torque must be balanced by the torque created by the front loading and drove the pickup head to focus. In more detail, between the seesaw arm and the pins there is a rotary junction, which is comprised of a lateral. The function of limited working distance ($\pm$0.2 mm) that is less than the effective focal length (0.525 mm) is capable of avoiding any abrupt impacts on the head to damage the disk. The use of lubricating oil is necessary for the slip-on procedure. It theoretically increased the strength of the interface. However, it must be considered that the grease is normally dissipated after a few weeks. To resolve the mechanical lubrication and working noise, solid dry film lubrication coating provides permanent lubrication with consistent low

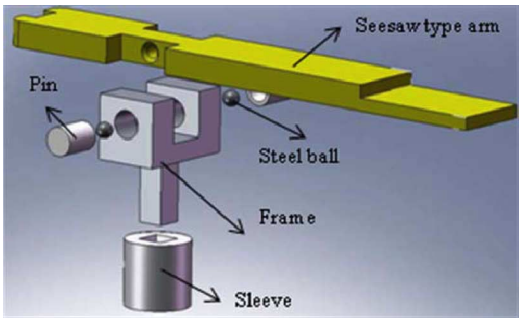

Fig. 4. Overall structure of seesaw type rotary VCM actuator.

friction performance over the coating lifetime. In the process of dry film coating, a dispersion layer of glue is applied to the pivot parts for low coefficient friction of seesaw motion to ensure life lubrication and low friction operation.

The overall structure of the seesaw actuator is shown in Fig. 4, which conforms to the small form factor device specifications. The seesaw arm was connected to two steel balls by the fixed cylinder pins. Cylinder pin restricts the ball rotation. The balls are designed specifically for rotating along one degree of freedom in X axis (with the direction of the pin clamped). When the driving force produces the moment around the axial base, the seesaw arm has a tilting motion in the focusing direction. The seesaw arm swiveling swinging effectively replaced the hinge spring vibration. The advantages of this design are as follows. Firstly, the total weight of the moving parts is lighter than that of any other parts of the actuator that has a hinge spring because leverage magnify the VCM driving force to achieve high effect focusing. Secondly, we adopt reinforcement such as aluminum alloy of light metal instead of triple layers of steel-aluminum-steel to increase the lateral stiffness. Also, the fabrication of triple layers is complex and expensive. Finally, the total mass of moving parts is counterbalanced in the seesaw arm's fulcrum, and the stress energy distribution is decreased to maintain the high sensitivity of the system.

In order to move the pickup head to the desired track, a VCM usually swings the optical pickup arm. The schematics of the conventional VCM are presented in Fig. 5(a). Generally, the magnetic circuit of the VCM actuator is composed of base yoke, and magnets. In the typical VCM, the magnet form is dual fan-shape with S and N poles in the right and left sides. The conventional VCM uses only vertically magnetized magnet. Magnets produce a magnetic flux to the voice coil. The yoke is made by high permeability materials such as nickel steel, silicon steel, etc. to confines the magnetic field. To meet the demands, it is desirable to make the flux denser to get the VCM driven force higher within the constraint of shape and air gap. High flux density in the air gap generates high actuating force and makes the seeking time shorter. The magnet circuit configurations of the multi-segmented magnet arrays (MSMA) VCM are shown in Fig. 5(b). However, the new type MSMA VCM contains magnet array that generated not only vertical magnetic field (Y-direction) for tracking but also horizontal magnetic field (X-direction) for focusing. The principle is that the magnetic field is concentrated on one side while diminished in the other side if X-directional magnets are combined with the Y directional magnet

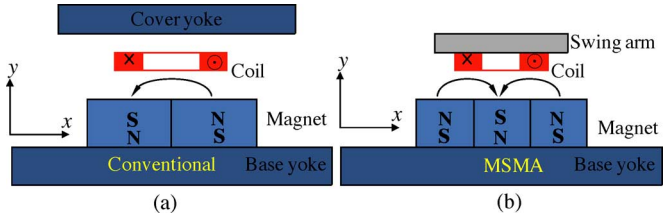

Fig. 5. Cross section of the VCM magnet array. (a) Conventional cross section. (b) MSMA cross section.

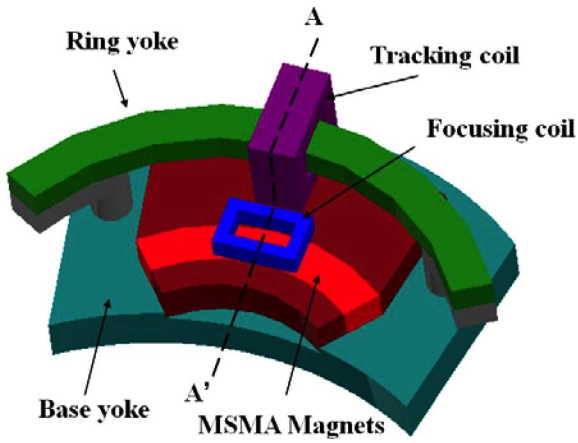

Fig. 6. MSMA VCM design of seesaw actuator.

array. MSMA structure has more magnetic flux exposed to the coil. This advantage showed apparently that MSMA in a swing arm type VCM provides higher flux density than conventional magnet array. This high flux density provides an opportunity for generating a larger driven force.

Several researches have shown that MSMA configuration in a swing arm type VCM provides a higher flux density and a larger actuating force than a conventional magnet array [20], [21]. The optical head can be moved faster and be more robust against disturbances by this feature. Our aim is to design a new VCM that can generate as much force as it can in the presence of the limited actuator size [22]–[24]. As shown in Figs. 6 and 7, we proposed the three layer MSMA magnet for reduction of out of plane force. The proposed design consists of ring yoke, base yoke, and fan-shape magnets. This design has three special features for reducing out-of-plane force. First, the actuating coil parts are placed above the edge of the MSMA magnets. This can decrease the force due to magnetic flux leaked from the edge. Second, the magnetic force distribution with ring yoke is more uniform and larger than the conventional design. We achieved the VCM design with small out of plane force and low cost. Third, the turns of voice coil was estimated from the magnetic parameters by considering inevitable air gaps for avoiding contact with the yoke and magnets. The particular ring yoke shortened the gap and reduced the coil turns effectively.

III. FE and EM Coupled Field Analysis and Simulation

The electromagnetic analysis for calculating the flux density in the air gap and in the yokes was carried out simultaneously by nonlinear 3-D finite-element method (FEM) Maxwell 9.0

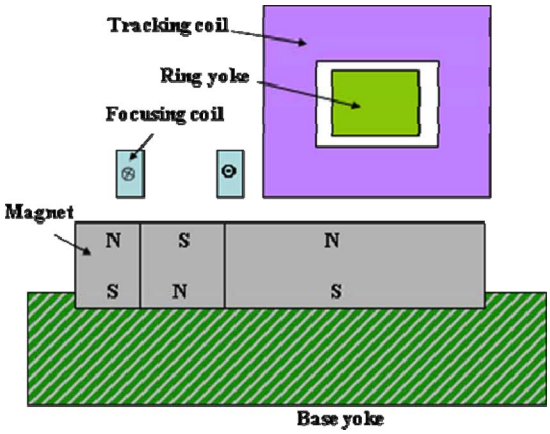

Fig. 7. A-A′ cross-sectional view for MSMA VCM.

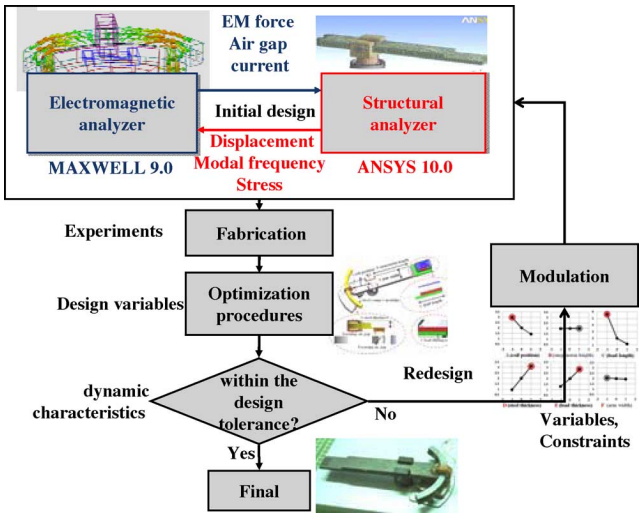

Fig. 8. Seesaw swing arm design flowchart based on FE and EM analysis.

[25]. The seesaw swing arm model is built by Ansys 10.0. Referring Fig. 8, since the simulation result of Maxwell 9.0 and ANSYS 10.0 can't be transferred and communicated directly between each other; we passed the results of each simulation to another analysis process for the dynamic characteristics to approach realistic models. Both FE and EM analyze results is required to conform the initial fabricated design measurement. If the deviation between simulation and measurement is within the design tolerance, we can assume that the data transfer between Maxwell 9.0 and Ansys 10.0 is effective. By considering all these design process, a final actuator model is suggested.

The FE model of 14 243 meshed elements with eight nodes is shown in Fig. 9. This design aspect is an overview of an actuator with small form factor optical pickup head to meet the actuator operating performance. The designated mechanical bandwidth of the seesaw arm type actuator is above 3 kHz and within 10 kHz. Referring to Figs. 10–12, the total five critical modes, from 0 Hz to 10 kHz are listed in Table II. The initial fabricated actuator did not satisfy the operating performance, and its servo bandwidth did not have the sufficient margin compared with the requirements. To avoid the degradation of the mobility by these modes, a seesaw arm for optical head should be designed for maximizing high enough frequency modes in lateral

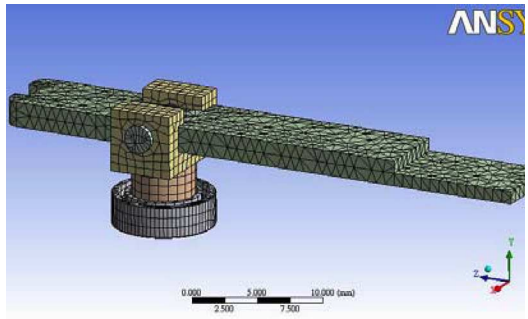

Fig. 9. FE model of seesaw type rotary VCM actuator.

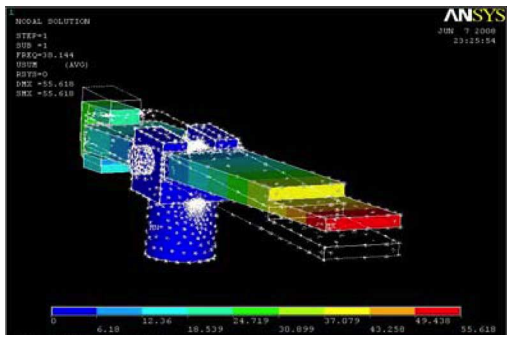

Fig. 10. Mode I cantilever resonance frequency: 38 Hz.

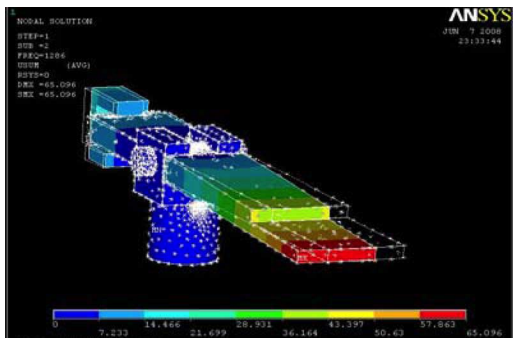

Fig. 11. Mode II first bending resonance frequency: 1285.6 Hz.

torsion and bending resonance. The torsion mode leads to optical aberration and out of focus. The first bending mode (1285.6 Hz) is restricted the tracking bandwidth, and the bandwidth of the focusing positioning is limited by the cantilever (38 Hz) and second bending mode (2531 Hz).

Parametric optimization investigates the behavior and the properties of swing arm structure under variations of the describing data (parameters). The optimal function for structure design factors is defined by

$$\max\left\{\left[F_{\text{focusing}}\cdot\left(\frac{1}{F_{\text{i. focusing}}}\right)\right]^2 + \left[F_{\text{tracking}}\cdot\left(\frac{1}{F_{\text{i. tracking}}}\right)\right]^2\right\} \quad (1)$$

where F_{focusing} is the cantilever mode frequency in the focusing direction, and F_{tracking} is the first bending mode frequency in

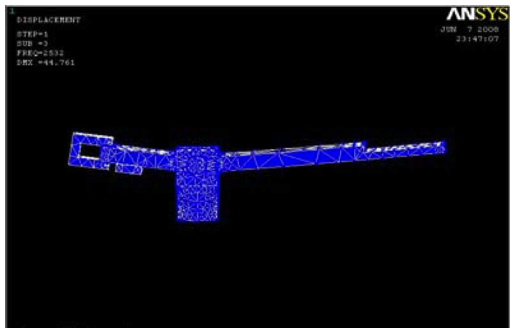

Fig. 12. Mode III second bending resonance frequency: 2531 Hz.

TABLE II
RESONANCE FREQUENCY MODES CHARACTERISTICS

Mode	Resonance frequency	Response
I	38 Hz	cantilever
II	1285.6 Hz	1st bending
III	2531 Hz	2nd bending
IV	5174 Hz	1st torsion
V	7648 Hz	2nd torsion

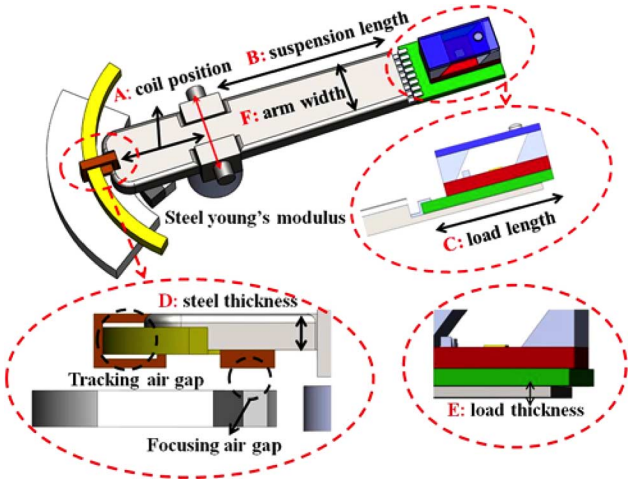

Fig. 13. Six design parameters candidates for operating optimization.

the tracking direction. $F_{\text{i. focusing}}$ and $F_{\text{i. tracking}}$ are the initial mode frequency without optimization process. Six major design parameters were selected in the optimal structural function parts as shown in Fig. 13. These parameters are selected as the most relevant control variables for the optimization of the seesaw actuator.

The relation between each design parameter and optimal function are shown in Fig. 14(a). The units in the range of -2 to 2 in the plots of Fig. 14 represent the percentile change of the model parameters A-F with respect to the initial model parameters A0-F0, in the range of -20% to 20%, respectively. The tolerance of six design parameters for initial dimension is shown in Table III. Therefore, it is concise to realize that the optimal function results changed with the parameters variation. Among these six parameters, parameters B and F (dash circle) were not included because they had low factors to influence the system efficiency. Therefore, a total of four parameters (A, C, D, and E) were used as design parameters to optimize the initial

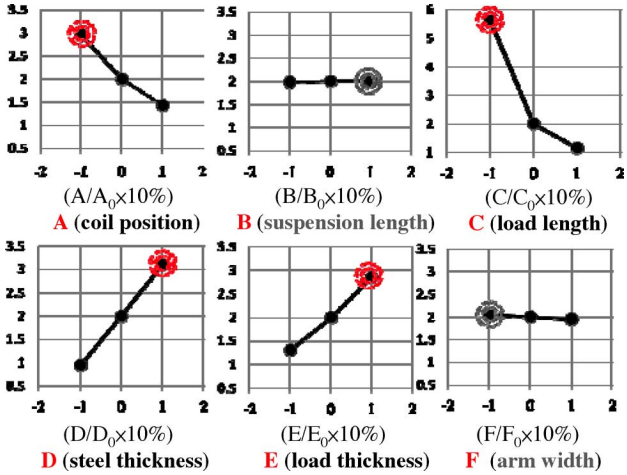

Fig. 14. Parametric optimization investigates the design parameters. (A) (coil position), (B) (suspension length), (C) (load length), (D) (steel thickness), (E) (load thickness), (F) (arm width).

TABLE III
THE TOLERANCE OF SIX DESIGN PARAMETERS

parameters	A	B	C	D	E	F
Initial(*mm*)	7	19	11	1.8	0.25	6.6
Upper bound(+*10%*)(*mm*)	6.3	17.1	9.9	1.62	0.225	5.94
Lower bound(–*10%*)(*mm*)	7.7	20.9	12.1	1.98	0.275	7.26

model and interactions of the system response. From a succession of optimization procedures, we acquired the optimized values of every design parameters. Selecting these optimized values, the mode frequencies were increased in the focusing and tracking direction. Consequently, the dynamic characteristics of the fabricated seesaw actuator were improved.

In the magnetic analysis using a commercial software Maxwell 9.0, the magnetic flux density distribution is computed in the regions of coils. To obtain force and the point movement, the following simulation procedure is necessary. The product of magnetic flux densities $\mathbf{B} = (B\_x, B\_y, B\_z)$ obtained in each nodes and current applied to the voice coil makes driving forces $\mathbf{f} = (f\_x, f\_y, f\_z)$ affecting on each nodes of the coil. The force component for each nodes of the coil can be obtained by

$$\begin{aligned} \mathbf{f} &= (f\_x, f\_y, f\_z); \\ \mathbf{I} &= (i\_x, i\_y, i\_z); \\ \mathbf{B} &= (B\_x, B\_y, B\_z); \\ \mathbf{f} &= n \cdot l \cdot (\mathrm{I} \times \mathbf{B}) \end{aligned} \tag{2}$$

where $\mathbf{f}$ = magnetic drive force; $\mathbf{I}$ = coil applied current; $\mathbf{B}$ = magnetic flux density; n = coil turns; l = effect length of coil. The magnetic distribution represents the vertical and horizontal dimensions of the focusing and tracking coils. The resultant force exerted inside the coil is expressed by

$$\mathbf{F} = \sum \mathbf{f}. \tag{3}$$

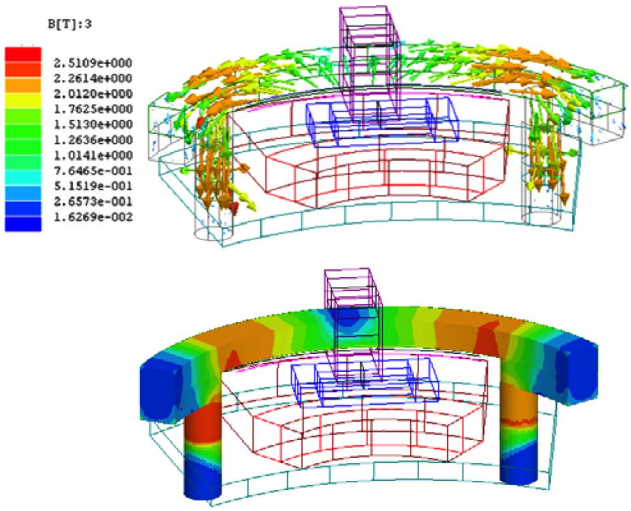

Fig. 15. 3-D EM model and magnetic flux lines on cross-sectional view of ring yoke.

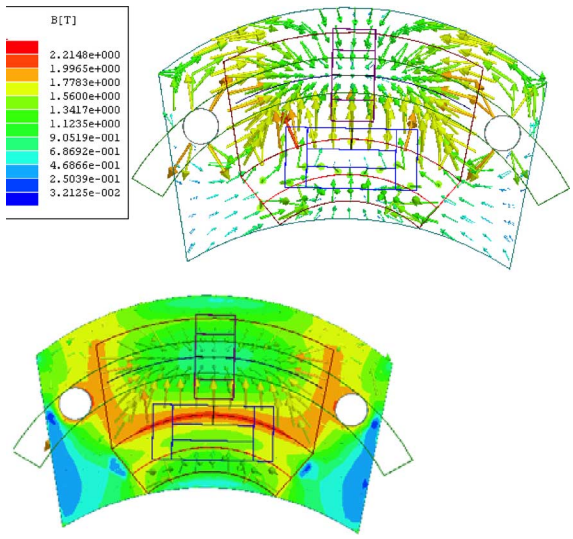

Fig. 16. 3-D EM model and magnetic flux lines on cross-sectional view of base yoke.

The MSMA design can let the magnetic forces uniformly distributed in the focusing and tracking coil, respectively. The simulation results of the 3-D Maxwell EM model of the ring yoke and base yoke are shown in Figs. 15 and 16. The relation between dynamic characteristics of actuator and the driving force generated by VCM is discussed next. We refer to the magnetic circuit design for suppressing mode vibration. The tracking and focusing coils, which are four hollow rectangular types, are attached to the seesaw arm moving part. Also, three fan-shape NdFeB magnets are combined with the base yoke. The yoke, the focusing coil, the tracking coils, and magnets form a magnetic circuit. Lorentz force is generated in this magnetic circuit, and drives the moving part in the focusing and tracking directions. As shown in Fig. 16, there is a ring yoke to obtain higher sensitivity by constituting more efficient magnetic circuit around tracking coils. The ring yoke conducted the magnetic flux which generated by the biggest fan-shape magnet in the array, and formed the vertical magnetic field for tracking operation. Due to the ring yoke constraint, the magnetic flux is uniform in the tracking coil, and the magnetic field intensity is strengthened to 0.505 Tesla even more. The peak of the first bending vibration mode follows the uneven magnetic flux density. Therefore, the uniform magnetic flux distribution in the tracking direction improves the seesaw actuator dynamic characteristics.

IV. Fabrication and Experiments

The new fabricated seesaw-shaped rotary VCM actuator is shown in Fig. 17. The seesaw arm is constructed of aluminum alloy to suppress magnetic influence between EM circuits. The sleeve in the middle of the seesaw arm was made from stainless steel, the yokes were made from carbon steel, and the magnets were made from NdFeB. Instead of the integrated pickup, a ballast mockup with the same mass was used for the dynamic tests and the target specifications of the actuator are shown in Table IV. In the experimental implementation, as shown in the Figs. 18 and 19, the relative displacement of the fabricated actuator is measured using a laser doppler vibrometer (LDV). A dynamic signal analyzer (DSA) records both input and output

Fig. 17. Fabricated seesaw swing arm VCM actuator.

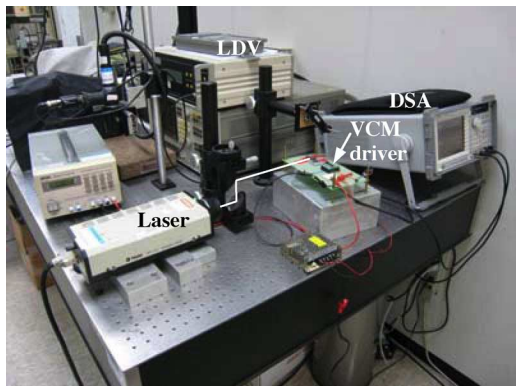

Fig. 18. Experimental apparatus.

signals of time-domain responses, and obtains the frequency responses of the VCM actuator.

The performance of the fabricated actuator was evaluated by dynamic experiments in the tracking and focusing direction. Fig. 20 shows the frequency response of the seesaw actuator. DC sensitivity is 0.194 mm/V and the cantilever mode frequency occurs at about 30 Hz. The Bode plot results shown the cantilever mode response tallied with the ANSYS simulation and had small resonance peak. The actuator we developed had a first bending mode of 3.85 kHz in focusing direction and is not noticeable in the Bode plot. However, in simulations, it had a

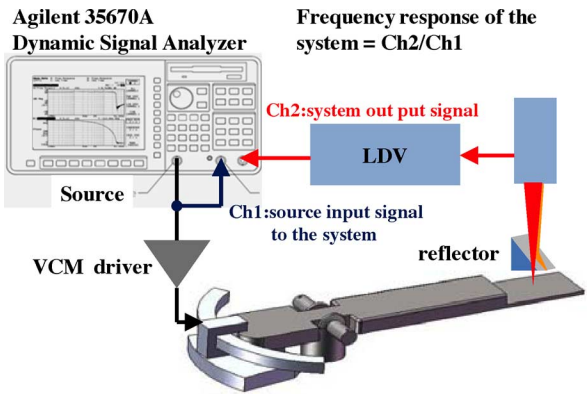

Fig. 19. Schematic of dynamic characteristics measurement.

TABLE IV
CHARACTERISTICS OF INITIAL MODEL

Total length (*mm*)	43.3	
Total width (*mm*)	6.1	
Total thickness (*mm*)	2.5	
Resistance of coil (Ω)	2.4	Focusing coil
	5.2	Tracking coil
Total mass (*g*)	2.08	Including bearing
DC sensitivity (*mm*/*V*)	0.194	

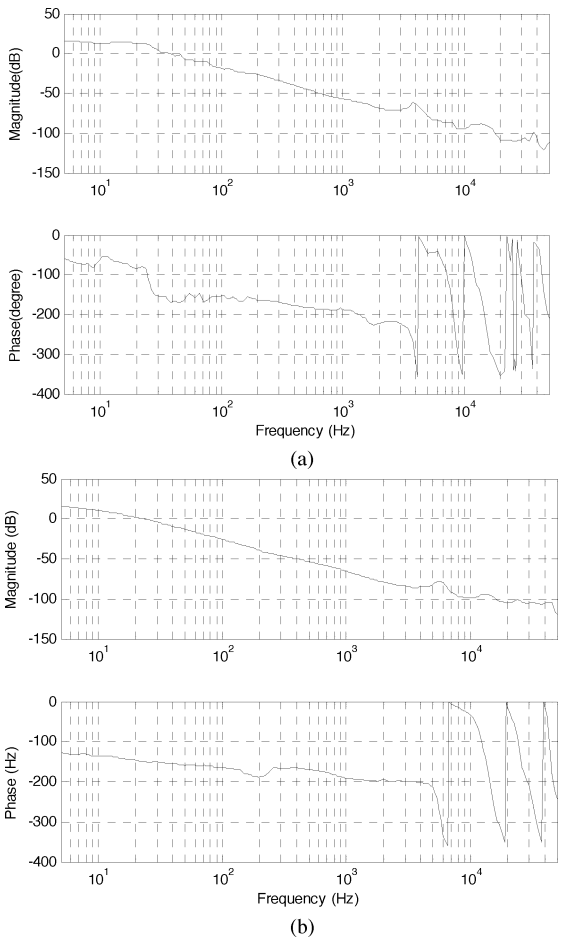

Fig. 20. The frequency responses of fabricated seesaw actuator. (a) Focusing direction. (b) Tracking direction.

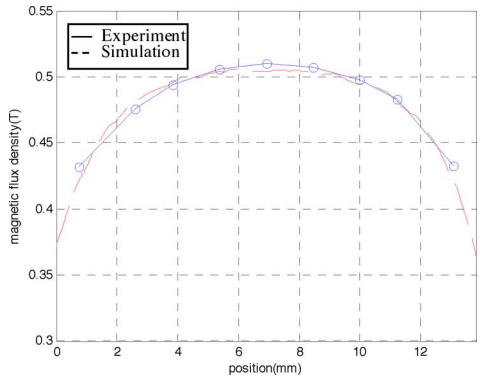

Fig. 21. The results of magnetic flux density measurement.

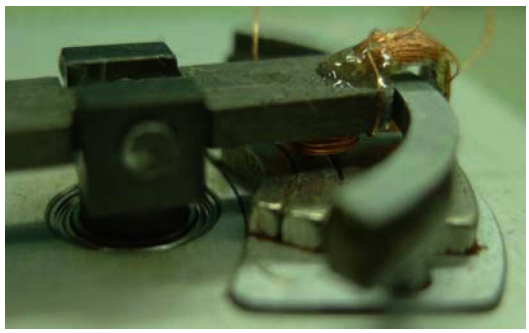

Fig. 22. Lateral view of MSMA circuit.

second resonance frequency of 4 kHz. This was caused by the faults of the manufacturing process using cutting tools and assembled conditions. If the actuator is fabricated by a technical method and it will have a sufficient first Bending mode frequency similar to the simulation.

A seesaw type mechanism with MSMA circuit was designed, manufactured, and evaluated in this study. To maximize the actuating force of the VCM within the limited actuator size, an optimal design process was employed for the actuator design. The dynamic characteristics of the manufactured actuator were measured, and its magnetic flux density for track seeking and focusing was evaluated. In the experiment, we used a digital Gauss meter (F.W. BELL 5180) to measure the magnetic flux density between the ring yoke and the MSMA magnets. Fig. 21 shows that the experimental results are met with the simulation. The maximum measured value of the normal flux density in the air gap is 0.505 T, and the boundary value is 0.43 T. Comparing the measured results with the simulation data, we find that the variation of the flux density is within 1%. However, the flux density at the center of the ring yoke reached 2.0 T and it was highly saturated at this point. The lateral view of fabricated fan-shape MSMA circuit is shown in Fig. 22. The thickness of magnet, base yoke, and ring yoke are 2.0, 1.4, and 1.5 mm, respectively. This high flux density performance provides adequate actuation force for driving small form factor optical devices.

V. CONCLUSION

For small form factor applications, a new seesaw swing arm actuator design for the integrated micro pickup head has been presented. This accurate lever mechanism magnifies focusing

force and strengthens the stiffness of load suspension. The effect of driving force on the actuator was studied to clarify the biaxial performance. The simulation with FE and EM analysis plays an important role in verifying the dynamic performance of the actuator and its magnetic flux distribution. An original seesaw actuator with MSMA magnetic circuit was specifically manufactured and assembled for a micro ODD. Natural frequencies of seesaw swing arm and MSMA magnetic force are measured to confirm the results of FE analyses. Furthermore, a parametric design modeling procedure was used to optimize the initial actuator dimensions and improve its components fabrication. The optimum parameters obtained, for enhancement of the resonance frequency modes, provided better dynamic characteristics of the fabricated seesaw actuator, which in turn validated the theoretical simulations. Experimental results were presented and discussed, demonstrating the performance of the actuator. Therefore, the proposed novel seesaw swivel structure is feasible for the small form factor high density optical storage system.

ACKNOWLEDGMENT

This work was supported by TDPA project 95-EC-17-A-07-S1-011, MOEA, and NSC project NSC 96-2221-E-009-149, Taiwan, R.O.C. The authors would like to thank the anonymous reviewers for useful comments and suggestions.

REFERENCES

[1] M.-G. Song, J.-H. Woo, N.-C. Park, J. Yoo, Y.-P. Park, and K.-S. Park, "Design of the rotary VCM actuator for small form factor optical disk drive," *Microsyst. Technol.* Mar. 17, 2009.

[2] D.-J. Lee, J.-H. Woo, S.-U. Kim, J.-S. Oh, J.-H. Yoo, N.-C. Park, Y.-P. Park, T. Shimano, and S. Nakamura, "Development of L-shaped rotary voice coil motor actuator for ultra slim optical disk drive using integrated design method based on coupled-field analysis," *Jpn. J. Appl. Phys.*, vol. 46, no. 6B, pp. 3715–3723, Jun. 2007.

[3] D.-J. Lee, S.-J. Park, J. Oh, N.-C. Park, Y.-P. Park, and H.-S. Jung, "Development of rotary-type voice coil motor actuator for small-form-factor optical disk drive," *Jpn. J. Appl. Phys.*, vol. 45, no. 2B, pp. 1124–1128, Feb. 2006.

[4] J. Jeong and D.-G. Gweon, "Optimal design of rotary-type voice coil motor using multi segmented magnet array for small form factor optical disk drive," *Jpn. J. Appl. Phys.*, vol. 46, no. 5A, pp. 2912–2914, May 2007.

[5] M. Sgwa and K. Aruga, "Evaluation system for residual vibration from HDD mounting mechanism," *IEEE Trans. Magn.*, vol. 35, no. 2, pp. 868–873, Mar. 1999.

[6] Y. Tang, S. X. Chen, and T. S. Low, "Micro electrostatic actuators in dual-stage disk drives with high track density," *IEEE Trans. Magn.*, vol. 32, no. 5, pp. 3851–3853, Sep. 1996.

[7] S.-J. Yoon, J. Lee, Y.-P. Park, and D.-H. Choi, "Design of optical flying head for magnetooptical recording," *IEEE Trans. Magn.*, vol. 41, no. 10, pp. 2851–2853, Oct. 2005.

[8] S. Kim, S.-J. Yoon, D.-H. Choi, and S.-Y. Lee, "A study on the flying stability of optical flying head on the plastic disks," *IEEE Trans. Magn.*, vol. 41, no. 2, pp. 986–988, Feb. 2005.

[9] R. J. Kadlec and C. R. Watt, "Focus Detection in a Digital Focus Servo System.," U.S. Patent 6 970 410 B2, Nov. 29, 2005.

[10] H.-F. Shih, C.-L. Chang, K.-J. Lee, and C.-S. Chang, "Design of optical head with holographic optical element for small form factor drive systems," *IEEE Trans. Magn.*, vol. 41, no. 2, pp. 1058–1060, Feb. 2005.

[11] D. L. Blankenbeckler, D. H. Davies, W. W. A. Dunford, B. W. Bell, Jr., and R. H. Hamer, "Performance characteristics of a 32 mm small form-factor optical disc and drive," *Jpn. J. Appl. Phys.*, vol. 43, no. 7B, pp. 4896–4899, Jul. 2004.

[12] Y. Chiu, H.-F. Shih, J.-C. Chiou, S.-T. Cheng, K.-Y. Hung, F.-G. Tseng, and W. Fang, "Design and fabrication of a small-form-factor optical pickup head," *IEEE Trans. Magn.*, vol. 45, no. 5, pp. 2194–2197, May 2009.

[13] E. J. Hong, D. W. Kim, N. C. Park, H. S. Yang, Y. P. Park, and S. K. Kim, "Design of swing arm type actuator and suspension for micro optical disk drive," *Microsyst. Technol.* pp. 1085–1093, Jul. 2005.

[14] E. J. Hong, W. S. Oh, N. C. Park, H. S. Yang, and Y. P. Park, "Design of suspension and swing arm for improved shock resistance in the micro optical disk drives," *Microsyst. Technol.* pp. 506–514, Jul. 2005.

[15] D. L. Blankenbeckler, B. W. Bell, Jr., K. Ramadurai, and R. L. Mahajani, "Recent advancements in DataPlay's small form-factor optical disc and drive," *Jpn. J. Appl. Phys.*, vol. 45, no. 2B, pp. 1181–1186, Feb. 2006.

[16] D. L. Blankenbeckler, B. W. Bell, Jr., D. H. Davies, and L. W. Lee, "An increased capacity DataPlay optical disc and drive," *SPIE* vol. 5380, pp. 171–181, 2004.

[17] F. Gao, F. F. Yap, and Y. Yan, "Modeling of hard disk drives for vibration analysis using a flexible multi-body dynamics formulation," *IEEE Trans. Magn.*, vol. 41, no. 2, pp. 744–749, Feb. 2005.

[18] H.-S. Lee, Y.-H. Kim, T.-Y. Hwang, and C.-S. Kim, "VCM design to improve dynamic performance of an actuator in a disk drive," *IEEE Trans. Magn.*, vol. 41, no. 2, pp. 774–778, Feb. 2005.

[19] D.-J. Lee, G.-W. Jung, N.-C. Park, H. S. Yang, Y.-P. Park, B. Y. Song, W. I. Cho, P. Y. Seong, and K. H. Lee, "Coupled-field-analysis and dynamic improvement of ultra slim optical pickup actuator," *Jpn. J. Appl. Phys.*, vol. 44, no. 5B, pp. 3373–3378, May 2005.

[20] J. Jeong, M. G. Lee, J.-H. Lee, H.-K. Yoon, and D.-G. Gweon, "Multi-segmented magnet array on voice coil motor in rotating data storage devices," *Jpn. J. Appl. Phys.*, vol. 43, no. 4A, pp. 1398–1402, Apr. 2004.

[21] M. G. Lee, J. Jeong, and D.-G. Gweon, "A comparative analysis of voice coil motors with multi-segmented and conventional magnet arrays for rotating data storage devices," *Jpn. Soc. Appl. Phys.*, vol. 42, no. 6A, pt. 1, pp. 3394–3395, Jun. 2003.

[22] C. Kaido, Nippon Steel Corp., "Effects of cores on the characteristics of an induction VCM," *IEEE Transl. J. Magn. Jpn.*, vol. 9, no. 6, pp. 1398–1402, Nov./Dec. 1994.

[23] H. Lin, Q. Li, Z. He, and S. Chen, "Development of a single coil coupled force VCM actuator for high TPI magnetic recording," *IEEE Trans. Magn.*, vol. 37, no. 2, pp. 850–854, Mar. 2001.

[24] M. A. Moser, "Shorted turn effects in rotary voice coil actuators," *IEEE Trans. Magn.*, vol. 32, no. 3, pp. 1736–1742, May 1996.

[25] J. R. Edwards, "Finite element analysis of the shock response and head slap behavior of a hard disk drive," *IEEE Trans. Magn.*, vol. 35, no. 2, pp. 863–867, Mar. 1999.